Check for updates

Unraveling the interaction between singlet state atomic oxygen O(^{1}D) and water: toward the formation of oxywater and hydrogen peroxide†

Jos Suijker[a] and Behnaz Bagheri [ID] ⋆[ab]

We performed high-level quantum mechanical calculations to explore the interaction of atomic oxygen in the ground triplet state, O(^{3}P), and the excited singlet state, O(^{1}D), with water. We reported the potential energy curves for a few lowest electronic states when an atomic oxygen approaches the oxygen of a water molecule. Our results predict the formation of a singlet oxywater species as the product of O(^{1}D) and H$_2$O which lies about 149.33 kJ mol^{-1} below the total energy of a singlet oxygen atom and a water molecule. Our calculations predict that an O(^{3}P) atom interacting with a water molecule forms a triplet oxywater complex with a shallow minimum on the triplet potential energy surfaces. We examined the transition of the singlet state oxywater species to hydrogen peroxide through the unimolecular reaction pathway, a (1,2)-hydrogen shift. We reported the structural properties, vibrational frequencies, and dipole moments of oxywater species, the transition state, and hydrogen peroxide. We also reported the energy barrier for the transition, and we provided an estimate for the respective reaction rate constant. In addition, we investigated the impact of solvents on the reaction pathway using an implicit solvation model of water. We predict that a singlet state oxywater species has a longer lifetime in a water environment than in the gas phase.

1 Introduction

Electric gas discharge plasmas generated in oxygen, O$_2$, containing gas mixtures, such as air or oxygen admixed with noble gases, produce atomic oxygen in either the ground triplet state, O(^{3}P), or the excited singlet state, O(^{1}D).[1–3] In contact with humidity or with aqueous solutions, oxygen atoms may undergo reactions with water molecules or may dissolve in solutions and undergo reactions in the liquid phase.[4–8] These reactions are crucial for the plasma processing of liquids and biological molecules for diverse applications in health and environmental remediation.[9,10] In addition, these reactions

are broadly involved in environmental chemistry and atmospheric chemistry.[11] Despite their significance, the detailed reaction mechanisms involving oxygen atoms in the presence of water are not completely understood. This motivates us to explore the interaction mechanisms between oxygen atoms and water molecules, with a particular emphasis on singlet state atomic oxygen, O(^{1}D).

Filatov *et al.*[12] were the first to consider the formation of oxywater, O·OH$_2$, theoretically by reaction of O(^{1}D) with water molecules

$$O(^1D) + H_2O \rightarrow O \cdot OH_2. \tag{1}$$
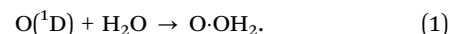
The authors used the complete active space self-consistent field, CASSCF, method to find the structure of oxywater at equilibrium and of the transition states. They also computed the energy to remove the oxygen atom from oxywater as 101.2 kJ mol^{-1} at the CASSCF level of theory and 107.16 kJ mol^{-1} at the multi-reference configuration interaction, MRDCI, level of theory.

Prior to the work of Filatov *et al.*,[12] a majority of experimental and theoretical studies on oxywater were focused on its potential existence as a structural isomer of hydrogen peroxide, H$_2$O$_2$, yielding controversial findings.[13–21] Bain and Giguère[13] made the first experimental reference to oxywater in which they concluded that any tautomeric form of hydrogen peroxide such

[a] *Department of Applied Physics and Science Education, Technical University of Eindhoven, PO Box 513, Eindhoven, 5600 MB, The Netherlands. E-mail: b.bagheri@tue.nl*
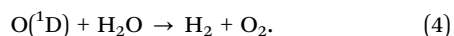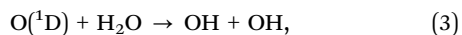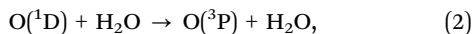
[b] *Institute for Complex Molecular Systems, PO Box 513, Eindhoven, 5600 MB, The Netherlands*

† Electronic supplementary information (ESI) available: Fig. S1 shows the potential energy curves for the O·OH$_2$ complex along the oxygen–oxygen coordinate from 1 Å to 10 Å for calculations wherein the geometry of H$_2$O is held fixed at each distance position. Fig. S2 depicts potential energy curves as an oxygen atom approaches the oxygen of a water molecule in calculations where the H$_2$O geometry is optimized at each distance position. In Fig. S3, the singlet potential energy curve is compared between calculations with H$_2$O held fixed and those with H$_2$O optimized at each distance position. See DOI: https://doi.org/10.1039/d4cp00969j

This journal is © the Owner Societies 2024

*Phys. Chem. Chem. Phys.*, 2024, **26**, 15277–15285 | 15277

as O·OH$_2$ was unlikely because they failed to observe O–O stretching other than the one which characterizes hydrogen peroxide. Theoretical studies of Pople *et al.*[16] suggested that oxywater does not exist as a stable minimum. However, theoretical studies of other authors in ref. 17–19 and 21 concluded that oxywater is a genuine minimum on the H$_2$O$_2$ potential energy hypersurface, and although oxywater may only have a transient existence in the gas phase, it is likely to be longer lived in protic solvents. Later, the experimental findings of Schröder *et al.*[20] suggested that oxywater is a viable molecule in the gas phase. After the investigation by Filatov *et al.*,[12] the rearrangement of oxywater into hydrogen peroxide with the assistance of water molecules was also studied by Okajima.[22,23] Studies by Ignatov *et al.*[24] suggested that the ice surface stabilizes the oxywater against the transition to hydrogen peroxide due to the formation of hydrogen bonds. In 2009, Franz *et al.*[25] theoretically investigated the production of singlet oxygen atoms by photo-dissociation of singlet oxywater. They reported the energies of a few lowest electronic singlet states of oxywater along with dissociation of the oxygen–oxygen bond into water and singlet oxygen using multiscale multireference second-order Møller–Plesset perturbation theory. Accordingly, the energy to remove one oxygen atom in the lowest singlet state was predicted to be 89.12 kJ mol^{-1}.[25] More recently and in the context of plasma interaction with water, Yusupov *et al.*[26] investigated the interaction of atomic oxygen with liquid water using ReaxFF molecular dynamics simulations wherein abstraction of a hydrogen atom from a water molecule was predicted with subsequent formation of two OH radicals. Verlackt *et al.*[27] predicted the formation of oxywater as a result of interaction of singlet states oxygen atoms with water using density functional tight binding (DFTB)-based molecular dynamics simulations which was stable for a simulation time of 10 ps. Xu *et al.*[28] predicted the formation of oxywater as the intermediate product in the interaction between the singlet state oxygen atom and water using density functional theory (DFT)-based molecular dynamics simulations. This was followed by the generation of hydrogen peroxide as the final product.[28]

In macroscopic fluid simulations of electric gas discharge plasmas,[29,30] often the following reaction channels between singlet state atomic oxygen, O(^{1}D), and water molecules have been considered:

$$O(^1D) + H_2O \rightarrow O(^3P) + H_2O, \tag{2}$$

$$O(^1D) + H_2O \rightarrow OH + OH, \tag{3}$$

$$O(^1D) + H_2O \rightarrow H_2 + O_2. \tag{4}$$

Channel 2 is a physical quenching process which deactivates the excited oxygen atom without any chemical change. The rate coefficient for this reaction is reported to be $k_1 = 1.2 \times 10^{-11}$ cm^3 molecule^{-1} s^{-1}.[31] Channel 3 was suggested in ref. 32–36 with a rate coefficient of $k_2 = (2.07 \pm 0.18) \times 10^{-10}$ cm^3 molecule^{-1} s^{-1} at room temperature using laser-induced fluorescence spectroscopy.[36] The rate coefficient of channel 4 relative to the rate coefficient of channel 3 is reported to be $k_3/k_2 \leq 0.016$.[37] The possibility of generating oxywater as a result of singlet state atomic oxygen interaction with water and its subsequent transition to a more stable product (*e.g.*, hydrogen peroxide) has not been considered in macroscopic simulations of electric gas discharge plasmas. In this work, we re-examined the mechanism of oxywater production as a result of atomic oxygen interaction with water molecules using high-level quantum mechanical calculations. We predict the production of a relatively stable singlet state oxywater species as a product of singlet state atomic oxygen interacting with water. We predict that the ground triplet state atomic oxygen interacting with a water molecule forms a triplet oxywater complex with a shallow minimum on the triplet potential energy curves. We also investigated the transition from the singlet state oxywater complex to hydrogen peroxide,

$$O(^1D) + H_2O \rightarrow O·OH_2 \rightarrow H_2O_2, \tag{5}$$
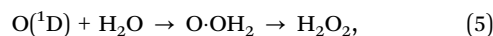
and we provide an estimate of the respective reaction rate constant. Furthermore, we explored the impact of the solvent environment (*i.e.*, water) on the reaction path using an implicit solvent model of water. We predict that the lifetime of the singlet oxywater species in the water environment is longer than that in the gas phase.

The rest of this manuscript is organized as follows: the methods are described in Section 2. It is followed by the results and discussion in Section 3. Finally, concluding remarks are presented in Section 4.

2 Methodology

We first used the complete active space self consistent field with 10 active electrons in 8 orbitals, (10,8)CASSCF, and the strongly contracted N-electron valence state perturbation theory,[38–40] SC-NEVPT2, to investigate the potential energy curve derived from atomic oxygen approaching the oxygen of a water molecule, commencing at a distance of 4.0 Å and gradually approaching the oxygen of the water (H$_2$O ← O). We used the correlation-consistent polarized valence triple-zeta, cc-pVTZ, basis set of Dunning and coworkers.[41,42] The molecular complex has C_{2v} symmetry at all positions of the potential energy curve. We conducted two sets of calculations: in the first set, the geometry of H$_2$O was held fixed at each oxygen–oxygen distance and all atoms were in one plane, while in the second set, the geometry of H$_2$O was optimized for each oxygen–oxygen distance.

In addition, we used the (10,8)CASSCF method and the coupled cluster methods, namely CCSD (including single and double excitations) and CCSD(T) (including single, double, and perturbatively treated connected triple excitations), all with the correlation-consistent polarized triple-zeta, cc-pVTZ, basis sets to explore the unimolecular reaction pathway of the oxywater species to hydrogen peroxide through the (1,2)-hydrogen shift. We also examined the effect of the solvent (*i.e.*, water) on the reaction pathway using an implicit solvation model of water with a dielectric constant of 80.4 and a refractive index of 1.33.

15278 | *Phys. Chem. Chem. Phys.*, 2024, **26**, 15277–15285

This journal is © the Owner Societies 2024

The latter was only applied to the CCSD and CCSD(T) methods using the conductor-like polarizable continuum model.[43] All the above procedures were carried out using the program ORCA[44] version 5.0.4.

3 Results and discussion

3.1 Formation of oxywater

The potential energy curve for the O·OH$_2$ complex along the oxygen–oxygen coordinate, from 1 Å to 4 Å, at the (10,8)CASSCF-SC-NEVPT2/cc-pVTZ level of theory is shown in Fig. 1. The lowest lying states on the triplet energy surface, ^{3}P, on the singlet energy surface, ^{1}D, and on the second excited energy surface, ^{1}S, are shown. The energies are plotted with respect to the energy of a H$_2$O molecule and an O(^{3}P) atom at an oxygen–oxygen distance of 10 Å (see Fig. S1 of the ESI,† for the energy curves in the 1–10 Å region). Additionally, a zoom of the triplet potential energy curves around the 3 Å region is shown in Fig. 2. In all these calculations, the geometry of H$_2$O at each oxygen–oxygen distance position was held fixed. The results wherein the geometry of H$_2$O at each oxygen–oxygen distance position is optimized are shown in Fig. S2 and S3 of the ESI.† In the latter case, the potential energy curves shift toward lower energies, while the overall features of the energy curves remain consistent. This outcome is expected, given the optimization of H$_2$O at each distance position. At an oxygen–oxygen distance of 10 Å, the energy gap between O(^{1}D) and O(^{3}P) is about 1.98 eV (about 191 kJ mol^{-1}) according to our calculations. This is in good agreement with the reported energy gap from the NIST database, which is about 1.97 eV.[45,46]

The product of a triplet oxygen atom O(^{3}P) and a H$_2$O molecule has a shallow minimum on the 3B$_1$ (1) and 3B$_2$ (1) energy surfaces at an oxygen–oxygen distance of about 2.75 Å
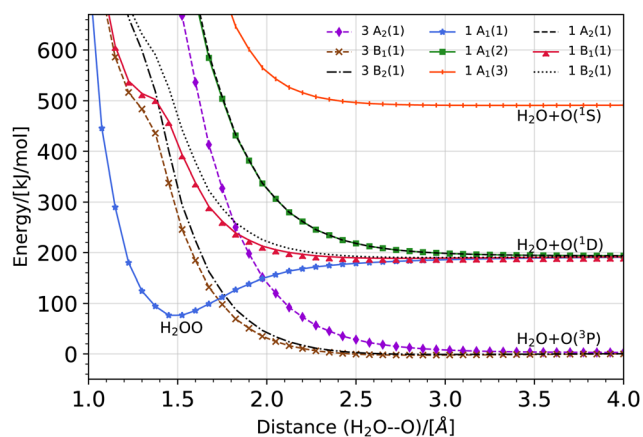

Fig. 1 Potential energy curve for the O·OH$_2$ complex along the oxygen–oxygen coordinate at the (10,8)CASSCF-SC-NEVPT2/cc-pVTZ level of theory. The lowest lying states on the triplet energy surface, ^{3}P, on the singlet energy surface, ^{1}D, and on the second excited energy surface, ^{1}S, are shown. The energies are plotted with respect to the energy of a H$_2$O molecule and an O(^{3}P) atom at an oxygen–oxygen distance of 10 Å (see Fig. S1 of the ESI,† for the energy curves in the 1–10 Å region). In these calculations, the geometry of H$_2$O is held fixed at each distance position.
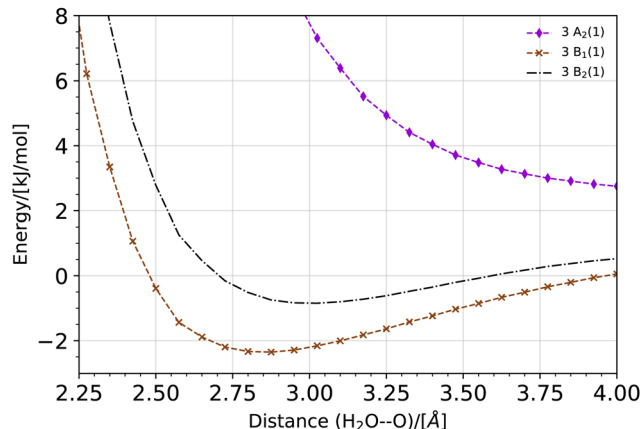

Fig. 2 Potential energy curve for the O·OH$_2$ complex along the oxygen–oxygen coordinate on the triplet energy surface, ^{3}P, at the (10,8)CASSCF-SC-NEVPT2/cc-pVTZ level of theory. The potential energy curve is shifted with regard to the total energy of a H$_2$O molecule and an O(^{3}P) atom at an oxygen–oxygen distance of 10 Å (see Fig. S1 of the ESI†). A zoom of the potential energy around a 3 Å oxygen–oxygen distance is shown. In these calculations, the geometry of H$_2$O is held fixed at each distance position.

leading to the formation of a triplet oxywater species, ^{3}O·OH$_2$, as shown in Fig. 2. This species may be viewed as a cluster stabilized by a weak electrostatic interaction between the apical oxygen and the hydrogens of the water molecule. The relative energies of the triplet oxywater species are about 2.41 kJ mol^{-1} below the total energy of a triplet oxygen atom and a water molecule on the 3B$_1$ (1) energy surface and 1.37 kJ mol^{-1} on the 3B$_2$ (1) energy surface. The appearance of the triplet oxywater species in our study is in agreement with studies by Filatov *et al.*[12] in which the triplet oxywater complex with an oxygen–oxygen distance of 3.002 Å at the (14,10)CASSCF/6-31G** level of theory was reported. Furthermore, the authors predicted that the relative energies of the triplet oxywater complex with respect to a triplet oxygen atom and a water molecule are 2.93 kJ mol^{-1} at the CASSCF level and 5.86 kJ mol^{-1} at the MR-(S)DCI level of theory.[12] The authors indicated that the obtained minimum may be due to the basis set superposition error (BSSE), and therefore, it may be an artifact of calculations.[12] It is challenging to determine the BSSE for such a complex using the CASSCF method as the complex as well as the isolate oxygen atom are in triplet states whereas the water molecule is in a singlet state. Therefore, the CASSCF space cannot be identical in different calculations needed for determining the BSSE. However, we examined the BSSE of the triplet complex at an oxygen–oxygen distance of 2.77 Å on the 3B$_1$ (1) energy surface for which we adapted the CASSCF space for an isolate triplet oxygen atom to (6,6)CASSCF, and for H$_2$O to (8,8)CASSCF while SC-NEVPT2 was still in use. With the calculated counterpoise correction, the binding energy was reduced by about 40% but it did not vanish. This suggests that the existence of a global minimum on the potential energy curve of the triplet complex may not be due to the BSSE. The 3A$_2$ (1) triplet energy surface does not lead to formation of a triplet

This journal is © the Owner Societies 2024

Phys. Chem. Chem. Phys., 2024, **26**, 15277–15285 | **15279**

oxywater species as the curve has only a repulsive feature (see Fig. 2).

As shown in Fig. 1, the product of the singlet oxygen atom $O(^1D)$ and the H_2O molecule has a minimum on the 1A$_1$ (1) energy surface at an oxygen–oxygen distance of about 1.5 Å, leading to formation of a relatively stable singlet oxywater species, $^1O\cdot OH_2$. The singlet oxywater species lies about 114.17 kJ mol^{-1} below the total energy of a singlet oxygen atom and a water molecule. By optimizing the H_2O molecule at each distance point, the singlet oxywater species lies about 149.33 kJ mol^{-1} below the total energy of a singlet oxygen atom and a water molecule (see Fig. S2 and S3 of the ESI†). In the latter calculation, by reducing the oxygen–oxygen distance from 1.1 Å to 1.0 Å, the energy of the singlet state, 1A$_1$ (1), remains almost unchanged (see Fig. S2, ESI†). At an oxygen–oxygen distance of $r(OO) = 1$ Å, the oxygen–hydrogen distance is $r(O_2H) = 1.57$ Å, the hydrogen–hydrogen distance is $r(HH) = 1.98$ Å, and the complex transitions to two separate hydrogen atoms while the two oxygen atoms are bonded (see Fig. 3 for the atomic numbering scheme used). Our results are in agreement with the studies of Filatov et al.[12] where it was predicted that the energy of the singlet oxywater complex is about 101.25 kJ mol^{-1} below the total energy of a singlet oxygen atom and a water molecule. Furthermore, our findings are in agreement with the studies of Franz et al.[25] who predicted a minimum on the singlet state energy curve at an oxygen–oxygen distance of about 1.64 Å with a depth of about 89.12 kJ mol^{-1} with respect to the total energy of a singlet oxygen atom and a water molecule at the MSMRMP2/TZVP level of theory. The remaining four singlet energy curves, 1A$_1$ (2), 3B$_2$ (1), 1A$_1$ (2), and 1B$_2$ (1), as well as the second excited state energy curve, 1A$_1$ (3), have repulsive characters (see Fig. 1).

In the following section, we explore the unimolecular reaction pathway of the singlet oxywater species to hydrogen

Fig. 3 Reaction diagram of the oxywater transition to hydrogen peroxide through the (1,2)-hydrogen shift calculated on the singlet energy surface at three different levels of theory, (10,8)CASSCF/cc-pVTZ, CCSD/cc-pVTZ, and CCSD(T)/cc-pVTZ, in a vacuum and in implicit water. The energies are relative to the energy of the oxywater species.

peroxide through the (1,2)-hydrogen shift. We also provide an estimate of the respective reaction rate both in a vacuum and in an implicit water environment. While explicit water molecules provide a more accurate description of molecular processes in water, the substantial computational cost associated with our quantum mechanical calculations necessitates this pragmatic approach.

3.2 Oxywater transition to hydrogen peroxide

We calculated the reaction pathway of the singlet oxywater species, $^1O\cdot OH_2$, to hydrogen peroxide through the (1,2)-hydrogen shift, at three different levels of theory, (10,8)CASSCF/cc-pVTZ, CCSD/cc-pVTZ, and CCSD(T)/cc-pVTZ, in a vacuum and in implicit water using the nudged elastic band (NEB) method.[47–49] The latter condition applies exclusively to the CCSD/cc-pVTZ and CCSD(T)/cc-pVTZ levels of theory. Fig. 3 depicts the energies of the transition state for (1,2)-hydrogen rearrangements, and the hydrogen peroxide relative to the energies of the oxywater species. The geometries of oxywater, hydrogen peroxide, and the transition state for the (1,2)-hydrogen shift were optimized at the three levels of theory in a vacuum and in implicit water, and are tabulated in Table 1. The atomic numbering scheme used in Table 1 is indicated in Fig. 3. The harmonic vibrational frequencies that are reported in Table 2 support our characterization of stationary points as minima and transition states on the potential energy surface. The predicted energies of hydrogen peroxide and the transition state relative to the energy of oxywater are provided in Table 4.

Structural properties. Our theoretical predictions of the structural properties of oxywater, the transition state, and hydrogen peroxide in a vacuum are in good agreement with those of Huang et al.[21] where the CCSD(T) methods with DZP and TZ2P+f basis sets were used, and those of Meredith et al.[19] where SCF, CISD, and CCSD methods with DZP, and TZ2P+f basis sets, and the CCSD(T) method with the DZP basis set were used. We included the structural properties of Huang et al.[21] at the CCSD(T)/TZ2P+f level of theory in Table 1 for comparison. To the best of our knowledge, oxywater has not been observed experimentally. However, hydrogen peroxide has been extensively studied, both experimentally and theoretically. Therefore, the extent to which our predictions for hydrogen peroxide align with experimental results can serve as an indicator of the potential success of our calculations in characterizing oxywater and the transition state. However, there has been a controversy over the equilibrium geometry of hydrogen peroxide due to its skew configuration which makes the determination of its four internal parameters from three rotational constants ambiguous. Therefore, a full set of internal parameters for hydrogen peroxide can only be obtained by selecting a value for one of the coordinates, which is usually the O–H bond length.[19,50] According to the infrared spectral data of Redington et al.,[50] the equilibrium geometry of hydrogen peroxide has a $r(O–O)$ distance of 1.475 Å, an angle of $\angle OOH$ of 94.8°, and a torsional angle of $\tau = 119.8°$ based on the assumption that the $r(O–H)$ distance is 0.950 Å which is in agreement with the torsional angle from the work of Oelfke and Gordy.[51] However, Koput[52]
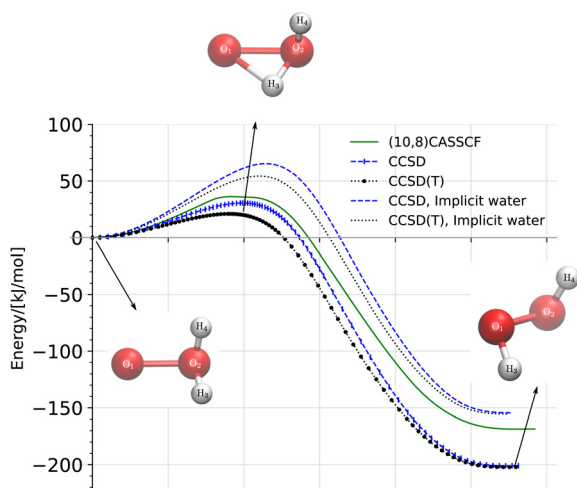
15280 | *Phys. Chem. Chem. Phys.*, 2024, **26**, 15277–15285

This journal is © the Owner Societies 2024

Table 1 Structural parameters of oxywater, the transition state, and hydrogen peroxide. Distances are in angstrom and angles in degree. The torsional angle, τ, is defined as $H_4–O_2–O_1–H_3$. The atomic numbering scheme used is indicated in Fig. 3

Structural properties	(10,8)CASSCF/ cc-pVTZ	CCSD/ cc-pVTZ	CCSD(T)/ cc-pVTZ	CCSD(T)/ TZ2P+f[a]	CCSD/cc-pVTZ implicit water	CCSD(T)/cc-pVTZ implicit water
Oxywater						
r(OO)	1.571	1.533	1.546	1.549	1.492	1.505
r(OH)	0.971	0.964	0.967	0.967	0.969	0.972
$\angle$ HOO	99.8	101.2	99.8	—	105.3	104.5
$\angle H_4O_2H_3$	107.4	109.5	108.4	106.4	111.7	110.7
Transition state						
r(OO)	1.641	1.610	1.628	1.634	1.585	1.600
$r(O_2H_4)$	0.972	0.964	0.967	0.968	0.969	0.972
$r(O_2H_3)$	1.046	1.032	1.023	1.031	1.065	1.062
$\angle H_4O_2O_1$	96.5	98.5	97.0	97.4	101.1	100.5
$\angle H_3O_2O_1$	55.0	57.1	59.4	—	54.4	55.4
$\angle H_3O_2H_4$	102.9	103.4	103.5	—	101.5	101.6
Hydrogen peroxide						
r(OO)	1.477	1.441	1.458	1.461	1.438	1.455
r(OH)	0.967	0.961	0.964	0.964	0.963	0.966
$\angle$ HOO	98.9	100.3	99.5	99.7	101.3	100.7
τ	116.7	113.1	113.9	111.9	99.0	99.6

[a] Data from the study of Huang et al.[21] for comparison.

Table 2 Theoretical vibrational frequencies (in cm^{-1}) for oxywater, the transition state for the hydrogen rearrangement, and hydrogen peroxide

Symmetry	(10,8)CASSCF/ cc-pVTZ	CCSD/ cc-pVTZ	CCSD(T)/ cc-pVTZ	CCSD(T)/ TZ2P+f[a]	CCSD/cc-pVTZ implicit water	CCSD(T)/cc-pVTZ implicit water	Assignment
Oxywater							
a'	688	704	672	666	816	791	O–O stretch
a''	961	874	830	848	984	973	O–O–H bend
a'	965	888	874	880	1024	993	Out-of-plane
a'	1698	1644	1627	1626	1637	1620	H–O–H bend
a'	3751	3788	3749	3741	3731	3697	O–H stretch
a''	3833	3885	3847	3840	3806	3770	O–H stretch
Transition state							
a	1340i	1217i	1059i	1103i	1557i	1439i	Reaction coordinate
a	698	698	680	670	756	738	O–O stretch
a	971	963	913	925	1064	1033	O–O–H bend
a	1510	1442	1467	1450	1346	1354	Out-of-plane
a	2959	3035	3094	3001	2813	2803	O–H stretch
a	3799	3840	3796	3788	3777	3734	O–H stretch
Hydrogen peroxide				Exp			
a	435	383	372	392	317[b]	371	354	Torsion
a	851	974	912	891	863[b], 864[c]	977	916	O–O stretch
b	1357	1357	1323	1322	1266[b], 1265[c]	1390	1355	O–O–H bend
a	1459	1468	1436	1426	1393[b]	1430	1397	O–O–H bend
b	3790	3850	3808	3801	3607[b]	3822	3782	O–H stretch
a	3840	3851	3809	3803	3608[b]	3829	3790	O–H stretch

[a] Theoretical data from the study of Huang et al.[21] [b] Experimental data from the study of Giguere and Srinivasan.[54] [c] Experimental data from the study of Hillman et al.[55]

obtained the following structure based on the assumption that the r(O–H) distance is 0.965 Å: r(O–O) = 1.464 Å, $\angle$ OOH = 99.4°, and τ = 111.8°. The experimental results of Koput[52] are in better agreement with our theoretical predictions. Additionally, our results for hydrogen peroxide are in good agreement with the theoretical predictions of Huang et al.[21] (see Table 1) and with those of Harding[53] using the *ab initio* anharmonic force field.

Theoretical vibrational frequencies. Our theoretical predictions of the vibrational frequencies, in particular the results of the CCSD(T)/cc-pVTZ method, are in reasonable agreement with the theoretical predictions of Huang et al.[21] at the CCSD(T)/TZ2P+f level of theory (see Table 2). In the case of hydrogen peroxide, the two methods demonstrate agreement within 1% for all frequencies, except for a 5% deviation in

This journal is © the Owner Societies 2024

Phys. Chem. Chem. Phys., 2024, **26**, 15277–15285 | **15281**

Paper

PCCP

torsion and approximately 2% variance in the O–O stretch. Similarly, for oxywater, the two methods align within about 1% for all frequencies, except for a discrepancy of approximately 2% in the O–O–H asymmetric bend. Experimental vibrational frequencies for hydrogen peroxide are available, enabling us to obtain a rough estimate of the validity of our theoretical predictions. The experimental values for hydrogen peroxide are considerably lower than our theoretical predictions. Scaling of our theoretical frequencies at the CCSD(T)/cc-pVTZ level of theory by a factor of 0.95 brings the O–H stretch within 0.3% of the experimental values, the O–O stretch within 0.3% of the experimental values, O–O–H bends within 0.7%, and the torsion within 11% of the experimental values. This suggests that our unscaled theoretical predictions for oxywater are also higher than the possible experimental results.

Theoretical dipole moments. Theoretical dipole moments (in Debye) for oxywater, the transition state, and hydrogen peroxide are presented in Table 3. Theoretical dipole moments are helpful in identifying these structures in experiments. The experimental dipole moment of hydrogen peroxide and the theoretical predictions by Huang et al.[21] are presented for comparison. For the dipole moment of hydrogen peroxide, our theoretical prediction using the (10,8)CASSCF/cc-pVTZ method is in excellent agreement with the experimental value. Using the CCSD(T)/cc-pVTZ (or CCSD/cc-pVTZ) method, the predicted dipole moment of hydrogen peroxide is about 11% (or 12%) smaller than the experimental value. Our theoretical predictions at the CCSD(T)/cc-pVTZ level of theory is about 2% smaller than the predictions of Huang et al.[21] at the CCSD(T)/TZ2P+f level of theory. The theoretical predictions of the dipole moment of oxywater are considerably large.

Energy barriers for oxywater transition to hydrogen peroxide. The relative energy of the transition state and hydrogen peroxide with respect to the energy of oxywater is presented in Table 4. The theoretical predictions by Huang et al.[21] at the CCSD(T)/TZ2P+f level of theory are shown for comparison. Hydrogen peroxide lies well below oxywater. Our results show that the activation barrier at the CCSD(T)/cc-pVTZ level of theory is about 3 kJ mol^{-1} smaller than those of Huang et al.[21] at the CCSD(T)/TZ2P+f level of theory. Our calculations in the implicit water environment predict a relatively higher energy barrier for the transition than that for the predictions in a vacuum. This suggests that the oxywater species is more stable in the water environment than vacuum. This result is in agreement with the results of Ignatov et al.[24] who suggested that the ice surface stabilizes the oxywater against the

transition to hydrogen peroxide due to the formation of hydrogen bonds. A similar conclusion can be made from the studies of Okajima[22,23] who theoretically investigated the formation of oxywater from hydrogen peroxide through the (1,2)-hydrogen shift mechanism and suggested that a protic solvent such as water can play a significant role in accelerating the formation of oxywater. Oxywater is a powerful oxidant against biomolecules especially in a hydrophilic environment.[22,23]

Reaction rate. We estimated the rate of the unimolecular reaction at room temperature (T = 298 K) using the following equation[57–59]

$$k(T) = \frac{k_B T}{h} \frac{Q^{TS}(T)}{Q^R(T)} \exp\left(-\frac{\Delta E_{act}}{k_B T}\right), \quad (6)$$

wherein k_B is the Boltzmann constant, T is the temperature, h is the Planck constant, and ΔE_{act} is the activation energy barrier. Q^{TS} and Q^R denote the total partition functions of the transition state and the reactant (i.e., oxywater for the forward reaction and hydrogen peroxide for the backward/reverse reaction), respectively. The total partition function includes contributions from all rotational states, Q_{rot}, and all vibrational states, Q_{vib}. In unimolecular reactions, the contribution from translational modes is not considered. Furthermore, at room temperature, the excited states remain unpopulated due to their relatively high excitation energies (see Fig. 1), allowing for the electronic contribution to be disregarded. Therefore, the total partition function is given by $Q = Q_{rot} \times Q_{vib}$. The rotational partition function is given by

$$Q_{rot} = \frac{\sqrt{\pi}}{\sigma_r}\left(\frac{8\pi^2 k_B T}{h^2}\right)^{3/2}\frac{1}{\sqrt{I_a I_b I_c}}, \quad (7)$$

wherein T is the temperature, and σ_r is the rotational symmetry (here is 1 as there is no centre of symmetry). I_i (i = a, b, c) is the principal moments of inertia for each rotational axis, and is attributed to the respective rotational frequency, ω_i, by $I_i = \frac{h}{8\pi^2 \omega_i}$. The vibration partition function is given by

$$Q_{vib} = \prod_{all\ vib}\left(1 - \exp\left(-\frac{h\nu_{vib}}{k_B T}\right)\right)^{-1} \quad (8)$$

in which the product operator is over all vibrational frequencies, ν_{vib}. The results at T = 298 K are presented in Table 5. As expected, hydrogen peroxide is a stable molecule and the backward reaction is almost absent with rates that are of the order of 10^{-23} (s^{-1}), 10^{-28} (s^{-1}), and 10^{-27} (s^{-1}) at the

Table 3 Theoretical dipole moments (in Debye) for oxywater, the transition state for the unimolecular rearrangement, hydrogen peroxide, and the experimental dipole moment for hydrogen peroxide for comparison

Species	(10,8)CASSCF/cc-pVTZ	CCSD/cc-pVTZ	CCSD(T)/cc-pVTZ	CCSD(T)/TZ2P+f[a]	CCSD/cc-pVTZ implicit water	CCSD(T)/cc-pVTZ implicit water	Exp.
Oxywater	4.68	4.58	4.52	4.54	5.71	5.31	
Transition state	3.25	3.17	3.24	3.15	3.70	3.74	
Hydrogen peroxide	1.58	1.78	1.76	1.80	2.60	2.46	1.58[b]

[a] Theoretical data from the study of Huang et al.[21] [b] Experimental data from the study of Cohen and Pickett.[56]

15282 | Phys. Chem. Chem. Phys., 2024, **26**, 15277–15285

This journal is © the Owner Societies 2024

Table 4 Energies (kJ mol^{-1}) of the transition state and hydrogen peroxide relative to the energy of oxywater

Species	(10,8)CASSCF/ cc-pVTZ	CCSD/ cc-pVTZ	CCSD(T)/ cc-pVTZ	CCSD(T)/ TZ2P+f^a	CCSD/cc-pVTZ implicit water	CCSD(T)/cc-pVTZ implicit water
Oxywater	0.0	0.0	0.0	0.0	0.0	0.0
Transition state	35.7	30.6	20.9	23.9	65.3	54.3
Hydrogen peroxide	−168.5	−200.9	−202.1	−195.8	−154.4	−155.5

^{a} Theoretical data from the study of Huang et al.[21]

Table 5 Reaction constants, k (s^{-1}), for the oxywater transition to hydrogen peroxide (forward) and the reverse (backward) reaction at T = 298 K

(10,8)CASSCF/cc-pVTZ	CCSD/cc-pVTZ	CCSD(T)/cc-pVTZ	CCSD/cc-pVTZ implicit water	CCSD(T)/cc-pVTZ implicit water
Forward reaction				
3.02×10^6	2.72×10^7	1.34×10^9	2.18×10^1	1.91×10^3
Backward reaction				
1.06×10^{-23}	1.55×10^{-28}	4.75×10^{-27}	1.89×10^{-26}	1.04×10^{-24}

(10,8)CASSCF/cc-pVTZ, CCSD/cc-pVTZ, and CCSD(T)/cc-pVTZ levels of theory, respectively. The rates of the forward reaction for hydrogen peroxide production are about 3.02×10^6 (s^{-1}), 2.72×10^7 (s^{-1}), and 1.34×10^9 (s^{-1}) at the (10,8)CASSCF/cc-pVTZ, CCSD/cc-pVTZ, and CCSD(T)/cc-pVTZ levels of theory, respectively. In general, the predicted rate is quite sensitive to the predicted value of the activation energy barrier. The rates of the forward reaction for hydrogen peroxide production in the implicit water environment reduce to 2.18×10 (s^{-1}) and 1.91×10^3 (s^{-1}) at the CCSD/cc-pVTZ and CCSD(T)/cc-pVTZ levels of theory, respectively. This suggests that oxywater is more stable in the water environment, which is in agreement with predictions of Ignatov et al.[24] and Okajima[22,23] that the oxywater species has a longer lifetime in water.

It is worth mentioning that because the three triplet potential energy curves arising from O^3 (P), 3B$_1$ (1), 3B$_2$ (1), and 3A$_2$ (1) cross the well of the singlet potential energy curve of the O·OH$_2$ complex, 1A$_1$ (1), there may be possible routes to deactivate the electronic excitation of the oxygen atom (see Fig. 1). In particular, the energy difference between the minimum of the singlet O·OH$_2$ well, the 1A$_1$ (1) state, and the 3B$_1$ (1) state at the crossing point is about 21.5 kJ mol^{-1}. The energy difference between the minimum of the singlet O·OH$_2$ well, the 1A$_1$ (1) state, and the 3B$_2$ (1) state at the crossing point is about 45.8 kJ mol^{-1}. These energy differences are within the range of the activation energy barrier toward hydrogen peroxide production (see Table 4) which suggests that there may be competition between production of the triplet oxygen atom and hydrogen peroxide formation if the spin–orbit coupling is strong enough.

4 Conclusions

Atomic oxygen either in the ground triplet state, O(^{3}P), or in the excited singlet state, O(^{1}D), can be produced by electric gas discharge plasmas generated in O$_2$ containing gases. We explored the interaction of O(^{3}P) and O(^{1}D) with water molecules. In particular, we examined the formation of the oxywater species as the reaction product of atomic oxygen and

water molecules. Our high-level quantum mechanical calculations predict the formation of a relatively stable oxywater species as the product of O(^{1}D) and H$_2$O. The energy of this singlet state oxywater complex is well below the total energy of a singlet O(^{1}D) atom and a water molecule (about 114.17 kJ mol^{-1} or 149.33 kJ mol^{-1}). We also predict a triplet oxywater complex as the product of the O(^{3}P) atom and the water molecule. The energy of the triplet oxywater complex is about 2.41 kJ mol^{-1} or 1.37 kJ mol^{-1} below the total energy of O(^{3}P) and H$_2$O.

Considering the singlet state oxywater species as a stable complex, we examined its transition to hydrogen peroxide through the unimolecular reaction pathway, the (1,2)-hydrogen shift. Our predicted structural properties, vibrational frequencies, and dipole moments are consistent and are in agreement with those of Huang et al.[21] The energy barriers for the transition to hydrogen peroxide are predicted to be about 35.7 kJ mol^{-1} at the (10,8)CASSCF/cc-PVTZ level, 30.6 kJ mol^{-1} at the CCSD/cc-pVTZ level, and 20.9 kJ mol^{-1} at the CCSD(T)/cc-pVTZ level. Performing the calculations in an implicit water environment results in relatively higher energy barriers which suggest a longer lifetime of the singlet oxywater species in the water environment. This is aligned well with the predictions of Ignatov et al.[24] and Okajima.[22,23]

Although the oxywater species has not yet been detected experimentally, a reaction channel for the production of the oxywater species and thereby hydrogen peroxide in macroscopic models of electric gas discharge plasmas may be important for predicting the final concentration of hydrogen peroxide.

Data availability

The input files to perform the simulations are provided at DOI: **https://zenodo.org/doi/10.5281/zenodo.10630824**.

Author contributions

JS and BB carried out the simulations and data analysis. BB conceived and supervised the project. BB wrote the manuscript in collaboration with JS.

Conflicts of interest

The authors declare no competing interests.

Acknowledgements

References

1 T. Jaffke, M. Meinke, R. Hashemi, L. G. Christophorou and E. Illenberger, *Chem. Phys. Lett.*, 1992, **193**, 62–68.

2 R. Peyrous, *Ozone: Sci. Eng.*, 1990, **12**(1), 41–64.

3 S. Schröter, A. Wijaikhum, A. R. Gibson, A. West, H. L. Davies, N. Minesi, J. Dedrick, E. Wagenaars, N. De Oliveira and L. Nahon, *et al.*, *Phys. Chem. Chem. Phys.*, 2018, **20**, 24263–24286.

4 J. Benedikt, M. M. Hefny, A. Shaw, B. R. Buckley, F. Iza, S. Schäkermann and J. Bandow, *Phys. Chem. Chem. Phys.*, 2018, **20**, 12037–12042.

5 M. M. Hefny, C. Pattyn, P. Lukes and J. Benedikt, *J. Phys. D: Appl. Phys.*, 2016, **49**, 404002.

6 V. Jirásek and P. Lukeš, *Plasma Sources Sci. Technol.*, 2019, **28**, 035015.

7 Y. Gorbanev, J. Golda, V. Schulz-von der Gathen and A. Bogaerts, *Plasma*, 2019, **2**, 316–327.

8 B. Myers, E. Barnat and K. Stapelmann, *J. Phys. D: Appl. Phys.*, 2021, **54**, 455202.

9 D. O'connell, L. J. Cox, W. B. Hyland, S. J. McMahon, S. Reuter, W. G. Graham, T. Gans and F. J. Currell, *Appl. Phys. Lett.*, 2011, **98**(4), 043701.

10 X. Lu, G. V. Naidis, M. Laroussi, S. Reuter, D. B. Graves and K. Ostrikov, *Phys. Rep.*, 2016, **630**, 1–84.

11 J. M. Anglada, M. Martins-Costa, J. S. Francisco and M. F. Ruiz-Lopez, *Acc. Chem. Res.*, 2015, **48**, 575–583.

12 M. Filatov, W. Reckien, S. D. Peyerimhoff and S. Shaik, *J. Phys. Chem. A*, 2000, **104**, 12014–12020.

13 O. Bain and P. A. Giguère, *Can. J. Chem.*, 1955, **33**, 527–545.

14 U. Kaldor and I. Shavitt, *J. Chem. Phys.*, 1966, **44**, 1823–1829.

15 D. Cremer, *J. Chem. Phys.*, 1978, **69**, 4440–4455.

16 J. A. Pople, K. Raghavachari, M. J. Frisch, J. S. Binkley and P. V. Schleyer, *J. Am. Chem. Soc.*, 1983, **105**, 6389–6399.

17 R. D. Bach, J. J. McDouall, A. L. Owensby and H. B. Schlegel, *J. Am. Chem. Soc.*, 1990, **112**, 7065–7067.

18 R. D. Bach, A. L. Owensby, C. Gonzalez, H. B. Schlegel and J. J. McDouall, *J. Am. Chem. Soc.*, 1991, **113**, 6001–6011.

19 C. Meredith, T. P. Hamilton and H. F. Schaefer III, *J. Phys. Chem.*, 1992, **96**, 9250–9254.

20 D. Schröder, C. A. Schalley, H. Schwarz, N. Goldberg and J. Hrûsák, *Chem. – Eur. J.*, 1996, **2**, 1235–1242.

21 H. H. Huang, Y. Xie and H. F. Schaefer, *J. Phys. Chem.*, 1996, **100**, 6076–6080.

22 T. Okajima, *Can. J. Chem.*, 2001, **79**, 22–28.

23 T. Okajima, *J. Mol. Struct.: THEOCHEM*, 2001, **572**(1), 45–52.

24 S. K. Ignatov, P. G. Sennikov, H.-W. Jacobi, A. G. Razuvaev and O. Schrems, *Phys. Chem. Chem. Phys.*, 2003, **5**, 496–505.

25 J. Franz, J. S. Francisco and S. D. Peyerimhoff, *J. Chem. Phys.*, 2009, **130**(8), 084304.

26 M. Yusupov, E. Neyts, P. Simon, G. Berdiyorov, R. Snoeckx, A. Van Duin and A. Bogaerts, *J. Phys. D: Appl. Phys.*, 2013, **47**, 025205.

27 C. Verlackt, E. Neyts and A. Bogaerts, *J. Phys. D: Appl. Phys.*, 2017, **50**, 11LT01.

28 S. Xu, V. Jirasek and P. Lukes, *J. Phys. D: Appl. Phys.*, 2020, **53**, 275204.

29 Y. Sakiyama, D. B. Graves, H.-W. Chang, T. Shimizu and G. E. Morfill, *J. Phys. D: Appl. Phys.*, 2012, **45**, 425201.

30 D. S. Stafford and M. J. Kushner, *J. Appl. Phys.*, 2004, **96**, 2451–2465.

31 J. C. Person and D. O. Ham, *Int. J. Radiat. Appl. Instrum., Part C*, 1988, **31**, 1–8.

32 G. Paraskevopoulos and R. Cvetanović, *Chem. Phys. Lett.*, 1971, **9**, 603–605.

33 J. C. Tully, *J. Chem. Phys.*, 1975, **62**, 1893–1898.

34 G. Streit, C. J. Howard, A. Schmeltekopf, J. Davidson and H. Schiff, *J. Chem. Phys.*, 1976, **65**, 4761–4764.

35 E. J. Dunlea and A. Ravishankara, *Phys. Chem. Chem. Phys.*, 2004, **6**, 3333–3340.

36 K. Takahashi, Y. Takeuchi and Y. Matsumi, *Chem. Phys. Lett.*, 2005, **410**, 196–200.

37 R. Zellner, G. Wagner and B. Himme, *J. Phys. Chem.*, 1980, **84**, 3196–3198.

38 C. Angeli, R. Cimiraglia and J.-P. Malrieu, *Chem. Phys. Lett.*, 2001, **350**, 297–305.

39 C. Angeli, R. Cimiraglia, S. Evangelisti, T. Leininger and J.-P. Malrieu, *J. Chem. Phys.*, 2001, **114**, 10252–10264.

40 C. Angeli, R. Cimiraglia and J.-P. Malrieu, *J. Chem. Phys.*, 2002, **117**, 9138–9153.

41 T. H. Dunning Jr, *J. Chem. Phys.*, 1989, **90**, 1007–1023.

42 A. K. Wilson, T. van Mourik and T. H. Dunning Jr, *J. Mol. Struct.: THEOCHEM*, 1996, **388**, 339–349.

43 V. Barone and M. Cossi, *J. Phys. Chem. A*, 1998, **102**, 1995–2001.

44 F. Neese, F. Wennmohs, U. Becker and C. Riplinger, *J. Chem. Phys.*, 2020, **152**(22), 224108.

45 NIST, Basic Atomic Spectroscopic Data, **https://physics.nist.gov/PhysRefData/Handbook/Tables/oxygentable5.htm** [Accessed: (April 2024)].

46 J. Gallagher and C. E. Moore, *Tables of spectra of hydrogen, carbon, nitrogen, and oxygen atoms and ions*, CRC Press, 1993.

47 G. Mills, H. Jónsson and G. K. Schenter, *Surf. Sci.*, 1995, **324**, 305–337.

48 H. Jónsson, G. Mills, K. W. Jacobsen, B. Berne, G. Ciccotti and D. Coker, *Classical and quantum dynamics in condensed phase simulations*, 1998.

49 G. Henkelman and H. Jónsson, *J. Chem. Phys.*, 2000, **113**, 9978–9985.

50 R. L. Redington, W. Olson and P. Cross, *J. Chem. Phys.*, 1962, **36**, 1311–1326.

15284 | *Phys. Chem. Chem. Phys.*, 2024, **26**, 15277–15285

This journal is © the Owner Societies 2024

51 W. C. Oelfke and W. Gordy, *J. Chem. Phys.*, 1969, **51**, 5336–5343.

52 J. Koput, *J. Mol. Spectrosc.*, 1986, **115**, 438–441.

53 L. B. Harding, *J. Phys. Chem.*, 1989, **93**, 8004–8013.

54 P. Giguere and T. Srinivasan, *J. Raman Spectrosc.*, 1974, **2**, 125–132.

55 J. Hillman, D. Jennings, W. Olson and A. Goldman, *J. Mol. Spectrosc.*, 1986, **117**, 46–59.

56 E. Cohen and H. Pickett, *J. Mol. Spectrosc.*, 1981, **87**, 582–583.

57 H. Eyring, *Chem. Rev.*, 1935, **17**, 65–77.

58 D. G. Truhlar, B. C. Garrett and S. J. Klippenstein, *J. Phys. Chem.*, 1996, **100**, 12771–12800.

59 S. Canneaux, F. Bohr and E. Henon, *J. Comput. Chem.*, 2014, **35**, 82–93.

This journal is © the Owner Societies 2024

Phys. Chem. Chem. Phys., 2024, **26**, 15277–15285 | **15285**